Journal of Alloys and Compounds 585 (2014) 776–782

Contents lists available at ScienceDirect

Journal of Alloys and Compounds

journal homepage: www.elsevier.com/locate/jalcom

Spray deposition of Cu_2ZnSnS_4 thin films

M. Valdés *, G. Santoro, M. Vázquez

División Electroquímica y Corrosión, INTEMA, Facultad de Ingeniería, CONICET-Universidad Nacional de Mar del Plata, Juan B. Justo 4302, B7608FDQ Mar del Plata, Argentina

ARTICLE INFO

Article history:
Received 17 June 2013
Received in revised form 27 September 2013
Accepted 2 October 2013
Available online 14 October 2013

Keywords:
Spray pyrolysis
Cu_2ZnSnS_4
Kesterite
Thin films
Solar cells

ABSTRACT

Thin films of Cu_2ZnSnS_4 (CZTS) have been deposited on top of glass substrates using spray pyrolysis and aqueous precursors. The substrate temperatures ranged from 325 to 425 °C. The effect of a thermal treatment in sulfur vapor on the structural, morphological, and optical properties of CZTS films have been studied. X-ray diffractograms revealed the formation of polycrystalline CZTS films, where the crystalline degree increased with substrate temperature and with the use of sulfur during annealing. Raman maps show a homogenous distribution of the CZTS phase along the analyzed surface and a random distribution of a Cu_XS binary phase. Raman signals attributed to this secondary phase seem to be reduced after sulfurization. Band gap values vary between 1.3 and 1.5 eV. The sulfurization treatment has no significant effect on the composition of the deposits or on the band gap energy value. However, the crystallite size increased after annealing in sulfur. Films deposited at 425 °C presented a nearly stoichiometric composition, suitable optical properties and *p*-type conductivity. These materials are suitable for absorbent layers in solar cell fabrication, even in the as-deposited condition.

© 2013 Elsevier B.V. All rights reserved.

1. Introduction

Cu_2ZnSnS_4 (CZTS) is a quaternary semiconductor that has emerged as a potential absorber substitute for $CuInGaSe_2$ in photovoltaic devices. This material has excellent optical properties ($\alpha \sim 10^5\ cm^{-1}$) and a direct band gap value that matches well the solar spectrum ($1.4 \leqslant E_{gap} \leqslant 1.5$ eV). Furthermore, it does not contain toxic elements such as selenium or expensive and scarce ones as indium and gallium. Due to their excellent properties, CZTS films are being intensively studied and are promising for developing low-cost, highly efficient and environmentaly friendly solar cells [1,2].

Numerous techniques are being currently investigated to prepare CZTS films. Among them, non-vacuum techniques are crucial to achieve cost reduction in the production of thin film solar cells. The highest efficiency for a CZTS solar cell has been reported as 11.1% by Barkhouse et al. using a low-cost method based on the preparation of CZTS nanoparticles [3].

Spray pyrolysis is a versatile technique that has been used before for the deposition of thin films of many types of compounds [4]. Moreover, it is cost effective, it does not require high vacuum, it can be used for irregular geometries and it can be used even on top of flexible substrates.

Spray pyrolysis of CZTS films was first reported by Nakayama and Ito [5]. As-deposited films resulted in sulfur-deficient compositions, so that stoichiometric films could only be obtained after a high temperature treatment in H_2S. Since then, several studies have been reported focused in the preparation of CZTS films by spray pyrolysis [6–9], many of them from alcohol-based precursor solutions. Here, we aim at preparing high quality CZTS from aqueous solutions, where the stoichiometry can be optimized by a sulfurization treatment with sulfur vapor that avoids the use of toxic H_2S.

2. Experimental

2.1. Deposition of Cu_2ZnSnS_4 films

Cu_2ZnSnS_4 (CZTS) films were deposited by spray pyrolysis. Bare glass and glass coated with fluorine-doped tin oxide (FTO, from Pilkington TEC Glass, TEC 8, ~8 Ohms/sq) were used as substrates ($2 \times 2 \times 0.2\ cm^3$). Prior to the deposition, both substrates were cleaned successively in detergent and isopropylic alcohol solution in an ultrasonic bath. Later, the substrates were placed in a hot plate during 1 h to reach the temperature of the spray process (T_s). CZTS thin films were prepared at 325, 375, and 425 °C. The precursor solution was obtained mixing aqueous solutions of 0.02 mol/L of $CuCl_2$; 0.01 mol/L of $ZnCl_2$; 0.01 mol/L $SnCl_2$ and 0.12 mol/L of CH_4N_2S with a final volume of 100 mL and a pH of 1.5. The ratio of elements Cu/Zn/Sn/S in the precursor solution was 2/1/1/12, as an excess in thiourea is necessary to compensate for sulfur loss during deposition. Cu_2ZnSnS_4 is produced by the following reaction:

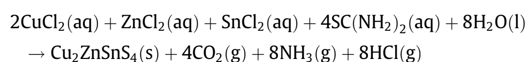

$$2CuCl_2(aq) + ZnCl_2(aq) + SnCl_2(aq) + 4SC(NH_2)_2(aq) + 8H_2O(l) \rightarrow Cu_2ZnSnS_4(s) + 4CO_2(g) + 8NH_3(g) + 8HCl(g)$$

During the spray, the solution was atomized through a glass nozzle using nitrogen as gas carrier. The spraying method used in this work was not continuous. A typical spray cycle comprised a spraying period of 30 s at 1.2 bars, followed by a 1 min pause between cycles. Immediately after the deposition, the hot plate was switched off so as to cool down the films. The deposition process was carried out under safety hood.

* Corresponding author. Tel.: +54 223 481 6600x244; fax: +54 223 481 0046.
E-mail address: mvaldes@fi.mdp.edu.ar (M. Valdés).

0925-8388/$ - see front matter © 2013 Elsevier B.V. All rights reserved.
http://dx.doi.org/10.1016/j.jallcom.2013.10.009

To improve the crystalline degree of the films, thermal treatments were carried out in a three-temperature zone thermal reactor. First, the samples were placed in the cold zone of the tube (room temperature). Then the second zone was heated to 500 °C and in the third zone the sulfur powder was allowed to reach 300 °C (melting started at around 200–250 °C). At this point, the samples were moved to the second zone in order to start the sulfurization process, as the vaporized sulfur got in contact with the samples assisted by argon flux. After 1 h the samples were cooled down by placing them back in the "cold zone".

2.2. Materials' characterization

The crystalline structure of the films was analyzed by X-ray diffraction in grazing incidence configuration (GXRD) using a PANalytical X'Pert PRO diffraction system employing Cu Kα radiation at 40 kV and 40 mA. The samples were scanned between 15° and 75°, with a step size of 0.01° and with the X-ray beam fixed at 3°. The crystallographic data for each phase were taken from the literature [10]. Alternatively, normal incidence (Bragg – Brentano, θ–2θ configuration) was used over a reduced 2θ interval, when XRD data were used to calculate the crystallite size. In this geometry the instrument contribution to the peak broadening was 0.124° calculated with a Si reference.

Raman spectroscopy measurements were performed using an Invia Reflex confocal Raman microprobe using a 50× objective. Excitation was provided with the 514 nm emission line of an Ar^+ laser. In this configuration the laser power on the sample was less than 2 mW measured with a silicon photodiode (Coherent Inc.). For this condition, no thermal effects could be detected as a result of recording the Raman spectra. Raman spectra were taken by averaging 3 acquisitions of 20 s each. Raman micro-mapping was performed scanning a square zone (80 × 80 μm) in the sample and recording 25 spectra in the x and y directions. For both axes the step between spectra was set in 20 μm.

The morphology and the chemical composition of the films were registered with a field emission scanning electron microscope (Carl Zeiss Supra 40 FESEM) coupled with an X-ray microanalysis system (Oxford Instrument, INCA processor). Cross-section images of the films were obtained using a Focused-Ion Beam Scanning Electron Microscope (Augira Cobra FIB SEM).

The thicknesses of sprayed CZTS films were measured using a KLA TENCOR D-100 profilometer.

A Shimadzu UV-160A spectrophotometer was employed to register absorption spectra in the wavelength range 500–1100 nm at room temperature and to calculate the band gap energy (E_{gap}) by extrapolation.

Photoelectrochemical measurements were carried out forming a semiconductor/electrolyte junction by immersion of the FTO/CZTS film in 0.2 mol L^{-1} Na_2SO_4 solutions. A three-electrode cell, with a Pt mesh as counter electrode and a saturated calomel electrode (SCE) as reference electrode, was used. The light source was a 150 W Xe lamp, chopped using an electronic shutter (UniblitzR model T132). A filter removes the ultraviolet radiation (Schott, λ < 350 nm). The light beam entered the cell through a quartz window and shinned on the film side of the glass. An IVIUM compact potentiostat/galvanostat was employed to carry out these measurements.

3. Results and discussion

3.1. Structural characterization

Fig. 1 displays GXRD patterns of CZTS films sprayed on glass substrates at different temperatures. For every temperature shown in Fig. 1a, diffraction planes match the standard XRD pattern of the Cu_2ZnSnS_4 phase (PDF file n° 26-0575). Unfortunately, in our experimental set-up, unfiltered Cu Kβ radiation produces spurious peaks. However these can be easily identified. The major diffraction peaks appear at $2\theta = 28.5°$, 47.4° and 56.2° which can be attributed to the (1 1 2), (2 2 0), and (3 1 2) crystallographic planes of CZTS. The (1 1 2) peak correlates better when the temperature increases, although the effect of temperature on the position of this peak is subtle. It has been shown before by other authors [11] that the intensity and resolution of XRD peaks are insufficient to distinguish kesterite from stannite, especially for thin polycrystalline films. However, stannite seems to be a more unstable phase for CZTS. The as-deposited films prepared at 325 and 375 °C present patterns with noisier, broader and less intense CZTS peaks than those obtained from samples deposited at a higher temperature (425 °C). This characteristic suggests that the crystalline degree increases when the films are deposited at higher temperatures. Furthermore, as-deposited samples prepared at 425 °C produce

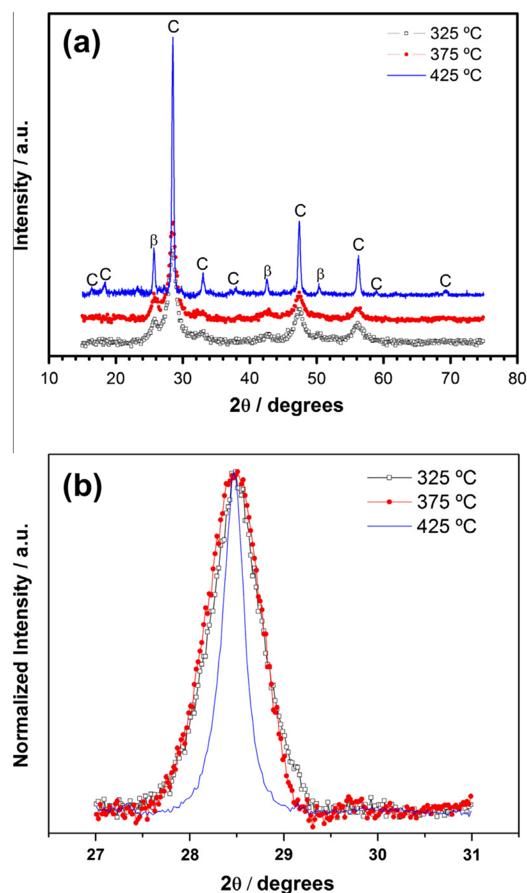

Fig. 1. XRD patterns of CZTS films sprayed on glass. (a) Grazing incidence XRD for films sprayed at different temperatures. Peaks labeled C denote CZTS diffraction planes while those labeled β are diffraction planes produced from unfiltered Cu Kβ radiation. (b) Normal incidence XRD restricted to the (1 1 2) diffraction plane used for crystal size calculation.

diffractograms that also show the lower intensity diffraction planes of CZTS phase (PDF file 26-0575).

In the case of quaternary compounds like CZTS, the presence of secondary phases can be expected. The most frequently found ones are binary compounds, such as Cu_xS in Cu-rich and ZnS in Zn-rich deposits as well as ternary phases such as Cu_2SnS_3 and $ZnSnO_3$. However, the results in Fig. 1 show no evidence of these secondary phases, even for as-deposited samples and independently of the hot plate temperature. However, ZnS with blend structure (PDF file 26-0566), exhibits some planes that are quite close to CZTS diffraction planes (1 1 2) and (2 0 0). For this reason, XRD results should be interpreted together with Raman spectra (see below) so as to achieve a better distinction between kesterite-type CZTS and ZnS structures.

The effect of an annealing treatment in S vapor atmosphere is shown in Fig. 2. Only one temperature is shown, although other temperatures produce similar results. In the case of Fig. 2a, the samples were deposited at 375 °C and the diffractogram was recorded using grazing incidence. It can be seen that after the sulfurization treatment the peaks become sharper, with a better definition in terms of the signal/noise ratio. Again, no peaks due to secondary phases are present in the diffractogram. Fig. 2b shows in detail the peak corresponding to the (1 1 2) plane using normal incidence. As-deposited and treated samples are compared at 325 °C. The intensity has been normalized to show that the signal becomes much sharper. The annealing treatment has little or no effect on the peak position. This appears to be in contrast with results of Yoo and Kim, who used a modified ultrasonic spray

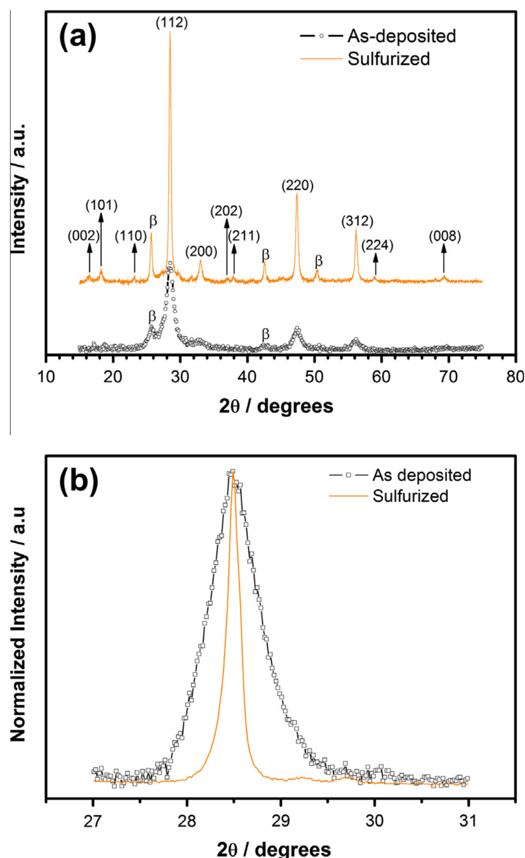

Fig. 2. Diffraction patterns of CZTS films sprayed on glass, with and without thermal treatment. (a) Grazing incidence XRD for films deposited at 375 °C. Diffraction planes labeled β are produced from unfiltered Cu Kβ radiation. (b) Normal incidence XRD restricted to the (1 1 2) diffraction plane used for crystal size calculation, for films deposited at 325 °C.

system and sulfurized for 30 min at 570 °C [12]. These authors found that after sulfurization *d*-spacing of sprayed CZTS film was restored, which they attributed to the relaxation of compressive stress.

The crystallite size (L) can be estimated from the full width at half maximum (FWHM) of diffraction peaks recorded at normal incidence and using Scherrer's formula [13–15]. Table 1 presents the crystallite size corresponding to the principal peak along the (1 1 2) plane. The values are in good agreement with those recently published by Shinde and col. [9]. As expected, the crystallite size increases after the thermal treatment. The increment is more notorious when the films are prepared in the low temperature range, probably due to the difference between deposition and sulfurization temperatures.

Due to its sensitivity, Raman spectroscopy is a useful technique to analyze the structure and the phase purity of CZTS samples. Besides, the presence of secondary phases likely to be formed during the deposition of CZTS can be masked by just using XRD analysis,

Table 1
Thickness (δ) of CZTS films calculated with profilometry and crystallite size (L) calculated with the principal peak along the (1 1 2) plane using Scherrer's equation (see Fig. 1b).

Temperature (°C)	Treatment	δ/μm	L/nm
325	As deposited	1.65	11.5
375	As deposited	1.61	10.8
425	As deposited	1.05	31.0
325	Sulfurized	2.00	82.3
375	Sulfurized	1.80	59.1
425	Sulfurized	1.35	62.6

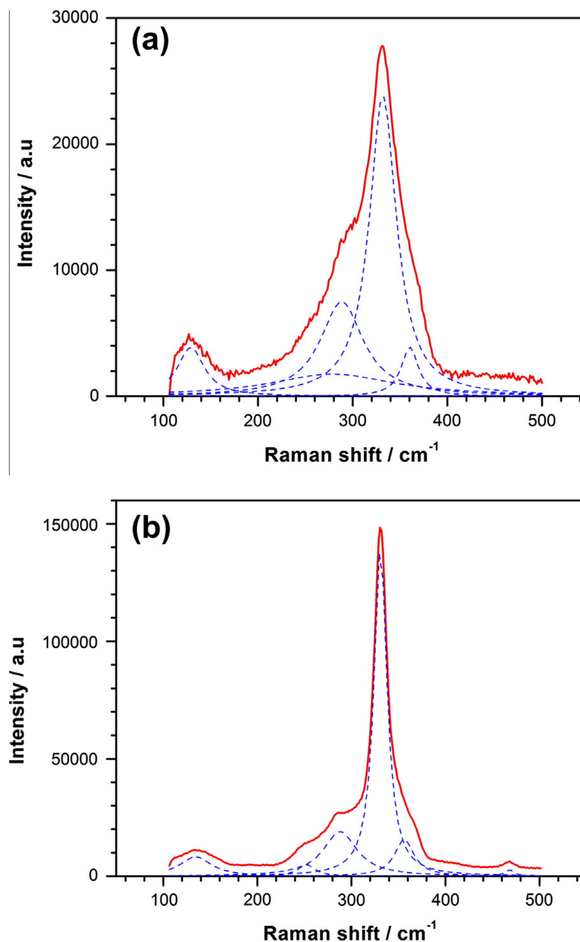

Fig. 3. Raman spectra of CZTS films sprayed on glass at different temperatures, (a) 325 °C and (b) 425 °C. The spectra were fitted using Lorentzian functions (dashed lines).

as commented above [16,17]. Fig. 3 presents Raman spectra of as-deposited CZTS films sprayed at two different temperatures; together with the fitting of the peaks using Lorentzian curves. The fitting procedure shows that each spectrum can be deconvoluted into several signals. Fig. 3a shows an average spectrum of samples deposited at low temperature (325 °C). As it can be seen, the spectrum is noisy and contains superimposed signals of relatively low intensity. The main band is dominated by two signals with peaks at 332 and 287 cm^{-1}. These signals are related to the two main vibrational modes of kesterite and both present A symmetry [18]. The signal at 332 cm^{-1} is blue-shifted in comparison to its calculated value at 335–337 cm^{-1}. This can be originated by residual stresses present in the film. Raman spectroscopy allows identifying stressed materials [19,20]. Fontané et al. have recently reported Raman results of CZTS films prepared by solid state reaction of pure elements [21]. For the first time, these authors report an unknown vibrational signal located at 331 cm^{-1} together with the A mode at 337 cm^{-1}. The authors related this signal to a local disorder in the cation sublattice, in agreement with the neutron diffraction data reported in similar samples [22]. The low crystalline degree showed by these as-deposited sprayed films can also be influenced by the contribution of local disorder in the cation arrangement. The spectrum in Fig. 3a also shows weaker contributions at 132, 255 and 360 cm^{-1} that can be attributed to low intensity E and B symmetry modes. Furthermore the signal located at 360 cm^{-1} is probably originated by the superposition of 350 and 370 cm^{-1} CZTS vibration modes [17]. Fig 3b presents the Raman spectrum of a sample deposited at 425 °C. Again, by fitting the

spectrum with Lorentzian curves, the same vibrational modes mentioned before are found to be present. Compared to that in Fig. 3a, the spectrum is less noisy and exhibits an improvement in the crystalline degree of the material, in agreement with GXRD results. A small signal located around 470 cm^{-1} is also observed and it is attributed to the presence of Cu_XS binary compounds [17,23]. Because this signal is not always present in every Raman spectrum, the distribution of this secondary phase will be analyzed using Raman micro-mapping.

The Full Width at Half Maximum (FWHM) decreases as the temperature increases (FWHM = 18 and 47 cm^{-1}), even if both values are typical of their relatively low crystalline nature.

Phase homogeneity and distribution were studied by Raman micro-maps presented in Fig. 4, where the effect of annealing in S vapor can also be seen. Fig. 4a–c shows Raman maps of sprayed CZTS films at 325, 375 and 425 °C respectively, without and with the sulfurization treatment. The effect of annealing is more noticeable at lower deposition temperatures (325 and 375 °C). After

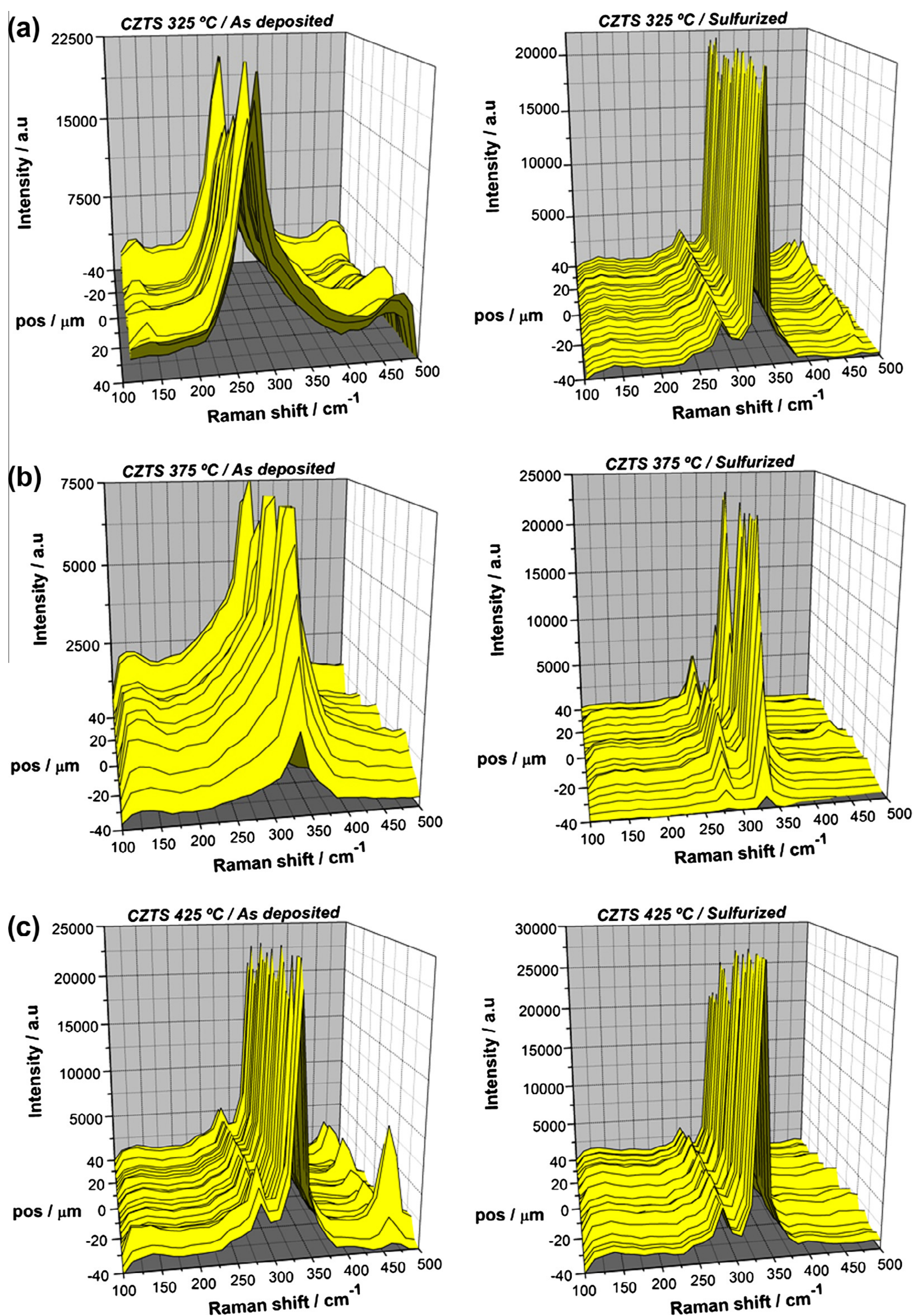

Fig. 4. Micro-Raman mapping performed over a 40 × 40 µm region of CZTS films sprayed on glass. (a) T_s = 325 °C; (b) T_s = 375 °C; (c) T_s = 425 °C. The effect of the sulfurization treatment is also shown for each T_s.

sulfurization CZTS Raman signals become sharper, the peaks are narrower which is indicating a higher crystallinity of the material, and the frequency of the main vibration modes is more defined. Furthermore the peak position of the A_1 mode shifts closer to the theoretical value of 336 cm^{-1}, and once more this effect is more noticeable in samples deposited at lower temperatures. The two main vibrational modes of kesterite with A symmetry (at 336 and 285 cm^{-1}) are now clearly separated into two peaks, as expected for more crystalline samples [24]. At 425 °C the difference in Raman spectra between as deposited and sulfurized films is negligible, which means that the crystalline degree of films deposited at 425 °C is high. This was also observed in GXRD measurements (not shown). The distribution of the CZTS phase along the film is homogeneous even in the as-deposited samples along the whole area under analysis, as indicated by the sharp signal at 332 cm^{-1}. The signal observed around 470 cm^{-1} originated by $Cu_{2-x}S$ compound presents irregular features. It is not always present in the spectra and its intensity and location fluctuate among the samples. From a statistical point of view, and on the basis of the intensity ratio between the A_1 and the $Cu_{2-x}S$ signal before and after the thermal treatment, it seems that the sulfurization treatment is beneficial to reduce the amount of this secondary phase. Normally copper sulfide undesired phases are removed by cyanide etching [25,26], so this approach can be employed to complete the removal of these compounds.

3.2. Morphology and composition

The morphology of as-deposited and sulfurized CZTS films is presented in Fig. 5 for samples prepared at two different temperatures. The images indicate that homogenous deposits were obtained in every case. No distinctive morphology is apparent even at high magnification. The rugosity seems to be higher for those samples prepared at low temperatures. The size of the grains seems to increase after annealing in sulfur, which is consistent with crystallinity improvement deduced from XRD results.

The cross section of the films was evaluated by FIB-SEM and resulted in average value of 1.45 μm (see Supplementary Information file). For the sake of comparison, thickness values of CZTS films determined by profilometry are shown in Table 1. The results from both techniques are in good agreement.

The chemical composition as a function of spray temperature for CZTS films was determined by EDS and is presented in Table 2. It can be observed that for as-deposited samples, the amount of copper in the film decreases while the sulfur content increases when the spray process is carried out at higher temperatures, so that both tend to their respective stoichiometric values. In contrast, the zinc content seems to deviate more from stoichiometry as the temperature increases, while the amount of Sn shows little effect of varying the temperature. When the films are sulfurized, EDS analysis reflects a minimal change in the elemental composition.

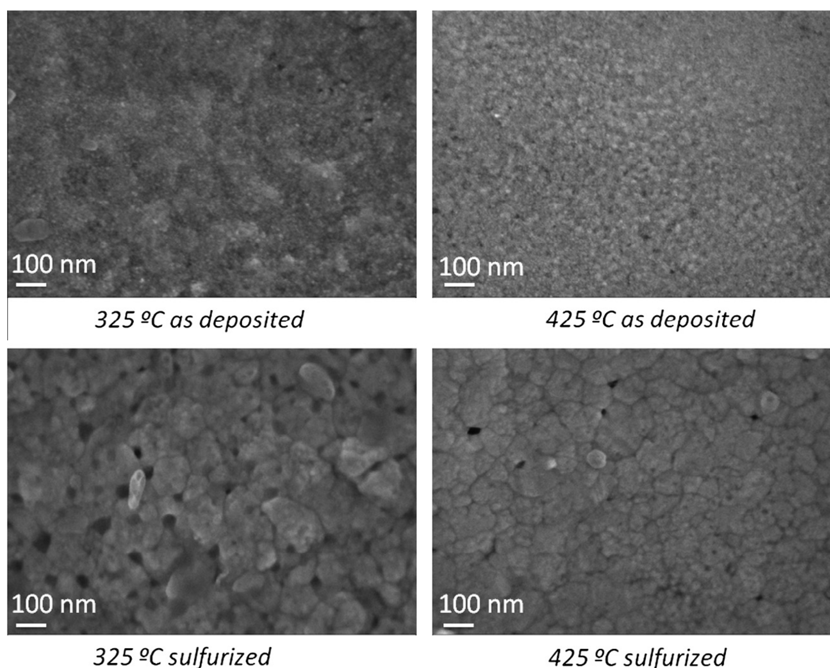

Fig. 5. FIB-SEM images of CZTS films sprayed (a and b) as-deposited and (c and d) sulfurized samples. (a–c) Samples prepared at 325 °C. (b–d) Samples prepared at 425 °C.

Table 2
Chemical composition of CZTS films obtained under various experimental conditions.

Condition	% Cu	% Zn	% Sn	% S	Cu/(Zn + Sn)	S/metal
Stoichiometric	25	12.5	12.5	50	1	1
T = 325 °C, as-deposited	26.68 ± 0.54	12.84 ± 0.06	13.38 ± 0.04	47.10 ± 0.16	1.02	0.89
T = 375 °C, as-deposited	25.14 ± 0.31	12.71 ± 0.19	13.17 ± 0.54	48.98 ± 0.43	0.97	0.96
T = 425 °C, as-deposited	25.50 ± 0.09	11.18 ± 0.22	13.50 ± 0.11	49.82 ± 0.02	1.03	0.99
T = 325 °C, annealed in Ar	28.42 ± 0.08	12.09 ± 0.01	12.88 ± 0.01	46.62 ± 0.08	1.14	0.87
T = 425 °C, annealed in Ar	26.66 ± 0.38	11.59 ± 0.18	12.60 ± 0.46	49.15 ± 0.66	1.10	0.97
T = 325 °C, annealed in S	24.34 ± 0.16	11.40 ± 0.81	12.40 ± 0.16	51.86 ± 0.82	1.02	1.08
T = 375 °C, annealed in S	24.82 ± 0.66	11.55 ± 0.55	12.43 ± 0.04	51.21 ± 0.08	1.04	1.05
T = 425 °C, annealed in S	23.23 ± 0.44	11.12 ± 0.25	13.10 ± 0.42	52.55 ± 0.23	0.96	1.11

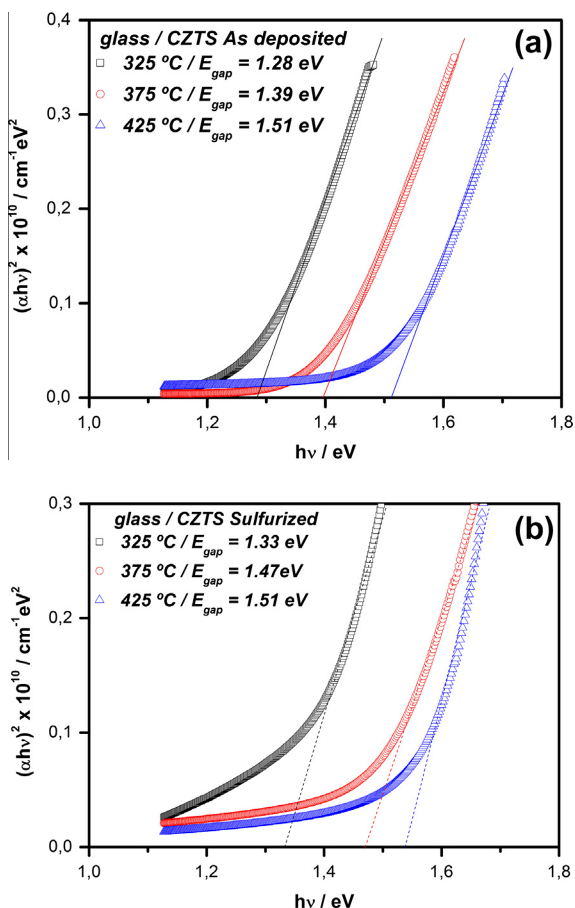

Fig. 6. Eg determination of CZTS films sprayed on glass at different temperatures. (a) as-deposited films and (b) sulfurized films. (□) T = 325 °C; (○) T = 375 °C; (Δ) T_s = 425 °C.

A thermal treatment in sulfur vapor does not seem to produce a better match to the stoichiometric composition. Taking all the conditions into account, those as-deposited samples prepared at 375 and 425 °C show a nearly stoichiometric composition.

3.3. Optical properties

In order to evaluate the band-gap energy, the absorbance of the CZTS films was measured over the wavelength range comprised between 500 and 1100 nm. When direct transitions are allowed, the absorption coefficient (α) has the following spectral dependence [27]:

$$\alpha h\upsilon = A(\alpha h - E_{gap})^{\frac{1}{2}}$$

where A is a constant and E_{gap} is the corresponding semiconductor band gap energy. Fig. 6 presents calculated band gap values for CZTS films sprayed on glass at different temperatures: as-deposited in Fig. 6a and after sulfurization in Fig. 6b. The optical band gaps calculated from these plots are within 1.3–1.5 eV, in good agreement with values reported by other authors [7,8,28,5]. As it can be seen, CZTS films deposited at low temperatures (325 °C) present low E_{gap} values, while films obtained at temperatures higher than 400 °C present band gap values which are in better agreement with previously reported experimental [29,30] and theoretical values [31,32] for this material. The sulfurization treatment seems to have little or no effect on the E_{gap} values. In any case, the band gap values of these CZTS films are suitable for their use in various photovoltaic and optoelectronic applications, such as solar cells. Other authors have obtained optical gaps within the range from 1.4 to 1.7 eV [6,5,33]. They attributed these somewhat large values to the presence of secondary phases such as $ZnSnO_3$, since this compound has a band gap of 2.42 eV.

Photoelectrochemistry has been employed to explore the semiconducting properties of CZTS. When semiconductor electrodes are exposed to periodic illumination, the current driven is affected by the creation of electron–hole pairs, which alters the concentration of minority carriers and thereby promotes processes governed by these carriers. During photoexitation both photopotential and photocurrent can be observed, even at open circuit potential. The photoexcited electrons and holes are separated in the space charge layer, and are driven by the electric field in opposite directions. This migration induces an inverse potential in the electrode (photopotential), reducing the potential difference across the space charge layer and retarding the migration of the carriers. In the case of p-type semiconductors, the Fermi level of the semiconductor decreases (the electrode potential increases) when the band edge level bends downward in the space charge layer. Moreover, a negative photocurrent is registered when photogenerated electrons move across the space charge region towards the electrode/electrolyte interface and increase the cathodic current [34]. Fig. 7 shows the photocurrent registered at open circuit potential and the photopotential developed across the junction for a CZTS sprayed at 425 °C. The cathodic nature of the photocurrent and the positive value of the photopotential confirm the p-type character of the film. Films deposited at lower temperatures were also p-type but they showed a smaller response.

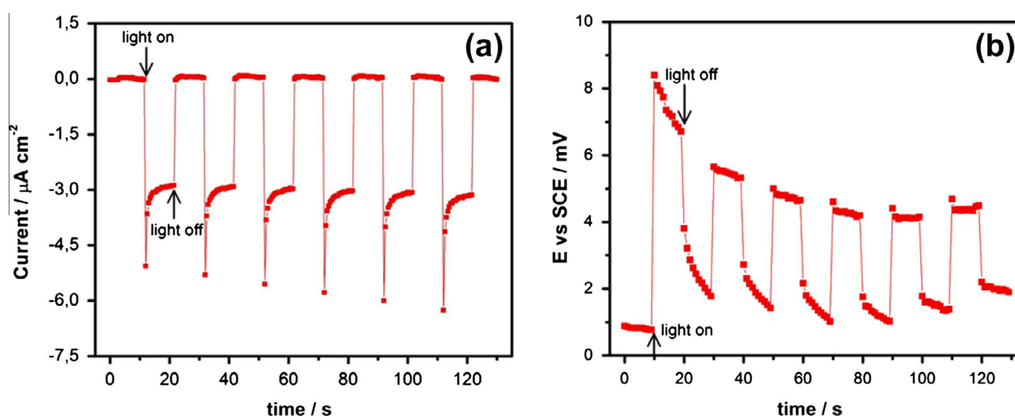

Fig. 7. (a) Photocurrent and (b) Photopotential response of sprayed CZTS thin film (T_s = 425 °C), using chopped light (10 s on/10 s off) in 0.2 mol L^{-1} Na_2SO_4 solution.

4. Conclusions

Cu_2ZnSnS_4 thin films have been successfully prepared by spray pyrolysis from an aqueous precursor. The effect of substrate temperature and sulfurization on the properties of the deposit was investigated. Structural characterization carried out using XRD and Raman spectroscopy indicated that CZTS is the dominant component; it is homogeneously distributed even on as-deposited samples. Raman mapping showed evidence of $Cu_{2-x}S$ in some spots, particularly when using the lowest temperature.

Deposited films have a nanocrystalline structure. For as-deposited samples, the crystalline degree improves when the films are prepared at high temperatures (425 °C), as shown by Raman and XRD. XRD and SEM analysis also show that the crystallite size increases after annealing in sulfur vapor from 10 to 30 up to 60–80 nm. This increment is particularly noticeable for films prepared at the lowest temperatures. The morphology is homogeneous but shows no characteristic feature, even at high magnification.

The optical band gap of the films ranged between 1.3 and 1.5 eV, in good agreement with reported values for CZTS prepared by different methods.

The sulfurization treatment has no significant effect on the elemental composition of the deposits or on the band gap energy value. However, the presence of binary, undesirable phases seems to be reduced after sulfurization.

Finally, CZTS films deposited at 425 °C present distinctive improvements when compared to films prepared at low temperatures. They show enhanced crystalline and physical properties, suggesting that when using appropriate parameters, spray pyrolysis can be taken as a promising technique to produce suitable CZTS absorber films for solar cells, even in the as-deposited condition. Current research is in progress to evaluate the performance of these films in CZTS solar cells prototypes.

Acknowledgement

Financial support from Consejo Nacional de Investigaciones Científicas y Técnicas (CONICET), Agencia Nacional de Promoción Científica y Tecnológica (FONCYT Project Code PICT 0110/11) and Universidad Nacional de Mar del Plata (UNMdP) from Argentina is highly acknowledged. The authors wish to thank to Dr. Thembela Hillie, from CSIR South Africa, for his assistance with FIB-SEM images; Dr. Mariela Desimone and Mr. Sebastián Rodriguez for their support in the XRD measurement.

Appendix A. Supplementary material

Supplementary data associated with this article can be found, in the online version, at http://dx.doi.org/10.1016/j.jallcom.2013.10.009.

References

[1] D.B. Mitzi, O. Gunawan, T.K. Todorov, K. Wang, S. Guha, Sol. Energy Mater. Sol. Cells 95 (6) (2011) 1421.
[2] S. Siebentritt, S. Schorr, Prog. Photovoltaics Res. Appl. 20 (5) (2012) 512.
[3] T.K. Todorov, J. Tang, S. Bag, O. Gunawan, T. Gokmen, Y. Zhu, D.B. Mitzi, Adv. Energy Mater. 3 (1) (2013) 34.
[4] P.S. Patil, Mater. Chem. Phys. 59 (3) (1999) 185.
[5] N. Nakayama, K. Ito, Appl. Surf. Sci. 92 (1996) 171.
[6] W. Daranfed, M.S. Aida, N. Attaf, J. Bougdira, H. Rinnert, J. Alloys Comp. 542 (2012) 22.
[7] M.A. Majeed Khan, S. Kumar, M. Alhoshan, A.S. Al Dwayyan, Opt. Laser Tech. 49 (2013) 196.
[8] N. Kamoun, H. Bouzouita, B. Rezig, Thin Solid Films 515 (15) (2007) 5949.
[9] N.M. Shinde, R.J. Deokate, C.D. Lokhande, J. Anal. Appl. Pyrolysis 100 (2013) 12.
[10] International Centre for Difraction Data (ICCD): Powder Difraction File Database, Newtown Square, EEUU, 1998.
[11] Y.B. Kishore Kumar, G. Suresh Babu, P. Uday Bhaskar, V. Sundara Raja, Sol. Energy Mater. Sol. Cells 93 (8) (2009) 1230.
[12] H. Yoo, J. Kim, Sol. Energy Mater. Sol. Cells 95 (1) (2011) 239.
[13] H. Araki, Y. Kubo, K. Jimbo, W.S. Maw, H. Katagiri, M. Yamazaki, K. Oishi, A. Takeuchi, Phys. Status Solidi C 6 (5) (2009) 1266.
[14] A.L. Patterson, Phys. Rev. 56 (10) (1939) 978.
[15] P. Scherrer, Göttinger Nachrichten Gesell 2 (1918) 98.
[16] X. Fontané, L. Calvo-Barrio, V. Izquierdo-Roca, E. Saucedo, A. Pérez-Rodriguez, J.R. Morante, D.M. Berg, P.J. Dale, S. Siebentritt, Appl. Phys. Lett. 98 (18) (2011) 56–89.
[17] P.A. Fernandes, P.M.P. Salomé, A.F. Da Cunha, J. Alloys Compd. 509 (28) (2011) 7600.
[18] T. Gürel, C. Sevik, T. Çağin, Phys. Rev. B: Condens. Matter Mater. Phys. 84 (20) (2011).
[19] V. Izquierdo-Roca, P.-R.A.A. Romano-Rodríguez, J.R. Morante, J. Álvarez-García, L. Calvo-Barrio, V. Bermudez, P.P. Grand, O. Ramdani, L. Parissi, O. Kerrec, J. Appl. Phys. 101 (10) (2007) 103517.
[20] A. Nakaruk, D. Ragazzon, C.C. Sorrell, Thin Solid Films 518 (14) (2010) 3735.
[21] X. Fontané, V. Izquierdo-Roca, E. Saucedo, S. Schorr, V.O. Yukhymchuk, M.Y. Valakh, A. Pérez-Rodríguez, J.R. Morante, J. Alloys Comp. 539 (2012) 190.
[22] S. Schorr, Sol. Energy Mater. Sol. Cells 95 (6) (2011) 1482.
[23] K.D. Lee, S.W. Seo, D.K. Lee, H. Kim, J.H. Jeong, M.J. Ko, B. Kim, D.H. Kim, J.Y. Kim, Thin Solid Films. 546 (2013) 294–298.
[24] M. Himmrich, H. Haeuseler, Spectrochim. Acta, Part A 47 (7) (1991) 933.
[25] B.A. Schubert, B. Marsen, S. Cinque, T. Unold, R. Klenk, S. Schorr, H.W. Schock, Prog. Photovoltaics Res. Appl. 19 (1) (2011) 93.
[26] J.J. Scragg, T. Ericson, X. Fontané, V. Izquierdo-Roca, A. Pérez-Rodríguez, T. Kubart, M. Edoff, C. Platzer-Björkman, Prog. Photovoltaics Res. Appl (in press) DOI: 10.1002/pip.2265.
[27] J.J. Tauc, Amorphous and Liquid Semiconductor, Plenum Press, New York, 1976.
[28] V.G. Rajeshmon, C.S. Kartha, K.P. Vijayakumar, C. Sanjeeviraja, T. Abe, Y. Kashiwaba, Sol. Energy 85 (2) (2008) 249.
[29] V.G. Rajeshmon, C.S. Kartha, K.P. Vijayakumar, C. Sanjeeviraja, T. Abe, Y. Kashiwaba, Sol. Energy 85 (2) (2011) 249.
[30] M. Patel, I. Mukhopadhyay, A. Ray, J. Phys. D: Appl. Phys. 45 (2012) 445103.
[31] S. Botti, D. Kammerlander, M.A.L. Marques, Appl. Phys. Lett. 98 (24) (2011).
[32] S. Chen, A. Walsh, J.-H. Yang, X.G. Gong, L. Sun, P.-X. Yang, J.-H. Chu, S.-H. Wei, Phys. Rev. B: Condens. Matter Mater. Phys. 83 (12) (2011) 125201.
[33] S. Das, K.C. Mandal, Conference Record of the IEEE Photovoltaic Specialists Conference, 2012, pp. 2668.
[34] N. Sato, Electrochemistry at Metal and Semiconductor Electrodes, Elsevier, Amsterdam, 1998.